J. Phys. G: Nucl. Phys. **10** (1984) 299–319. Printed in Great Britain

Silicon detectors and elementary particle physics†

P G Rancoita‡
EP Division, CERN, CH-1211 Geneva 23, Switzerland

Received 4 July 1983

Abstract. Silicon detectors are currently a major instrument in high-energy physics experiments. The analysis of their energy-loss data (whose deviation from the Landau–Vavilov theories has been studied recently) is performed to determine the decay point of short-lived $D\bar{D}$ particles. To use them in colliding beam machine experiments technological developments have been undertaken in order to achieve a large-scale integration for read-out chips. They can find application in calorimetry as a dense active sampling layer. The silicon sandwich calorimeters are well suited to operate near the vacuum pipes.

1. Introduction

Technological advances have enabled the construction of very thin, large size area silicon detectors and fast associated electronics. At present silicon counters are a major instrument in high-energy physics (for a review on the subject see Rancoita and Seidman (1982)). The development of thin-strip electrodes, the so called microstrip detectors, has yielded a resolution of approximately 5 μm (Hyams *et al* 1983). The new microstrip devices, whether or not associated with multilayer silicon targets, are intended to be employed in experiments for incoherent hadro- or photoproduction of charmed and beauty particles, since this physics requires high-resolution tracking devices in order to detect vertices which are closer to the interaction point.

The further increase in the active area of silicon detectors together with large-scale integration (LSI) (Bosman *et al* 1983 and see § 4) chips makes them attractive as inner vertex detectors in colliding beam machine experiments. The use of low-resistivity inexpensive silicon detectors has been investigated with a view to replacing scintillation counters in calorimetry (Barbiellini and Rancoita 1983), especially in magnetic environments or where there are geometric constraints or in vacuum pipes.

This paper presents a survey of the features of the detector and its applications in high-energy physics experiments. The trend of the development is discussed by considering the use of these detectors in forthcoming colliding beam machine experiments. Section 2 deals with the general characteristics of silicon devices, their associated electronics, data processing for multilayer targets and the modified energy-loss distribution. In § 3 the charge sharing between strips, the efficiency and the magnetic field effect in microstrip

† This paper was presented at The Institute of Physics Conference on Nuclear Structure and Elementary Particle Physics, Liverpool, 22–25 March 1983.
‡ CEN, Saclay, France (on leave from INFN, Milano, Italy).

0305-4616/84/030299 + 21 $02.25

detectors are considered. A survey of experiments at fixed-target and colliding beam machines is presented in § 4.

2. General characteristics

2.1. Silicon detectors and associated electronics

Silicon is the predominant semiconductor material used in production of radiation detectors. Detection of nuclear radiation is based on the process of ionisation or excitation of atoms in the detection medium by the passage of a charged particle (see § 2.2). The number of electron–hole (e–h) pairs produced by a relativistic particle in silicon is approximately $80\ \mu m^{-1}$.

Silicon detectors can be made very thin. The typical thickness used in high-energy physics varies between 100 and 500 μm. So far the devices employed have been of surface-barrier or ion-implanted type. Their resistivity is between 2 and 10 kΩ cm. The bulk silicon is usually n type. Surface-barrier detectors are made at room temperature by first etching the surface and then using an evaporated metal, usually gold, as the rectifying contact and aluminium as the ohmic one. Another method of creating junctions is to expose a silicon crystal to a beam of ions produced by an accelerator. This method is called ion implantation and can be used to form n^+ or p^+ layers by accelerating either phosphorus or boron ions respectively. The impurity concentration at the surface or at the most probable penetration depth (X_P) can be varied by varying either the ion bombardment energy or the angle of incidence during the implantation process. However, the impurity concentration has a tail extending up to $5X_P$. Compared with surface-barrier detectors, ion-implanted detectors are more stable and less subject to ambient conditions.

A new method of manufacturing silicon detectors (Kemmer 1980) based on a process (planar) which combines oxide passivation with ion implantation has been developed.

A great deal of development has led to hybrid and monolithic preamplifiers which are of low cost and (together with their associated receivers or amplifiers) have a fast response. In table 1 a simplified subdivision of electronic characteristics is presented as a function of the input capacitance to the preamplifier (the very large input capacitance refers to calorimetric application).

Recently, studies on radiation damage effects induced by relativistic particles have been carried out. The performance of ion-implanted detectors is degraded (i.e., a strong increase of the leakage current) after exposure to a fluence higher than that required to degrade a surface-barrier detector (Heijne 1981). In general, the lower the resistivity, the better the detector performance. A more specific investigation found that full depletion and full charge collection can be obtained by increasing the reverse bias voltage (Borgeaud *et al* 1983). In this way normal operations were obtained up to a fluence value of 8.31×10^{13} relativistic protons cm^{-2}.

Table 1. Characteristics of electronics.

Input capacitance (pF)	FWHM (noise) (keV)	Base time of signal (ns)
< 20	20	40
< 200	30	65
< 3000	150	1 μs

2.2. Multilayer silicon data and modified energy-loss distribution

Energy-loss data, namely the energy released in the detector, are recorded when the Si counters are the target and when they are arranged as a multilayer telescope along the beam direction (see § 4). A maximum likelihood analysis is usually performed in order to define the number of particles traversing each detector. In this way the position of the decay vertex of short-lived particles is reconstructed.

Let us now consider the simplest situation, namely a coherent reaction with only one short-lived particle decay inside the device (this method can be easily generalised to two decay vertices and incoherent reactions). To fit the decay position, X, one has to assume that n relativistic particles leave the production detector and that, from position X, m particles are present. Furthermore, we suppose that X is located in between the layers j and $j+1$. The likelihood function $L(X, n, m)$ (Rancoita and Seidman 1982) is just the product of the differential probabilities of obtaining the energy loss actually measured, assuming that the decay occurred at position X, and we have

$$L(X, n, m) = \Pi_{i=1,j} \Lambda(\Delta_i, n) \Pi_{i=j+1,f} \Lambda(\Delta_i, m) \tag{1}$$

where $\Lambda(\Delta_i, p)$ is the probability density of getting the energy loss Δ_i actually measured in the ith detector, assuming that p relativistic particles cross it; f is the total number of detectors and j is the first device after the production detector. Once the likelihood function is defined we have to consider its logarithmic function $l(X, n, m)$,

$$l(X, n, m) = -2 \ln L(X, n, m), \tag{2}$$

which has the significance of a χ^2 function (Rancoita and Seidman 1982). The best estimates for X (the position of the decay point), n (the number of particles produced in the interaction) and m (the number of particles after the decay) are given by the values of X, n and m for which l is minimum.

In order to evaluate the likelihood function $L(X, n, m)$ correctly, a precise knowledge of the energy-loss distribution is required.

The silicon detectors commonly employed have to be considered as thin absorbers, whereas the statistical nature of the ionisation process on the passage of a fast charged particle results in large fluctuations of the energy loss.

The energy straggling function, $f_{\mathrm{L,V}}(x, \Delta)$, is the solution of the transport equation

$$\frac{\partial f_{\mathrm{L,V}}(x, \Delta)}{\partial x} = \left(\int_0^b \omega'(\varepsilon') f_{\mathrm{L,V}}(x, \Delta - \varepsilon') \, \mathrm{d}\varepsilon' - f_{\mathrm{L,V}}(x, \Delta) \int_0^{E_\mathrm{m}} \omega'(\varepsilon) \, \mathrm{d}\varepsilon \right) x^{-1} \tag{3}$$

where $\omega'(\varepsilon) = (\xi/\varepsilon^2)[1 - \beta^2(\varepsilon/E_\mathrm{m})]$ is the Rutherford cross section for a free electron, E_m is the maximum transferable energy in a collision, $\xi = 153.4(z^2/\beta^2)(Z/A)x\rho$ keV $= 5.35/\beta^2$ keV for a charged particle traversing 300 μm of silicon, z and βc are the charge and velocity of the incoming particle, ε is the actual energy transferred in a collision and x is the thickness of the absorber in cm.

Landau (1944) solved equation (3) by using a Laplace transform method and assuming $b = E_\mathrm{m} = \infty$. The Landau distribution is given by

$$f_\mathrm{L}(x, \Delta) = (1/\xi)\varphi(\lambda)$$

where $\varphi(\lambda) = (1/2\pi\mathrm{i}) \int_{r-\mathrm{i}\infty}^{r+\mathrm{i}\infty} \exp(u \ln(u) + \lambda u) \, \mathrm{d}u$ and r is an arbitrary real positive constant. The function $\varphi(\lambda)$ is a universal function of the dimensionless variable λ,

$$\lambda = (1/\xi)(\Delta - \langle\Delta\rangle) - \beta^2 - \ln(\xi/E_\mathrm{m}) - 1 + C = (1/\xi)[\Delta - (\Delta_\mathrm{mp} - \xi\lambda_0)],$$

where C is the Euler constant (0.577 215), λ_0 is the value for which φ is a maximum and Δ_{mp} is the most probable energy loss for the Landau distribution. The function $\varphi(\lambda)$ has been tabulated by Boersch-Supan (1961). The full width at half maximum (FWHM) of the Landau distribution is approximately 4ξ. The parameter ξ has the meaning of an energy scale parameter.

In the Vavilov (1957) solution of equation (3), the correct maximum transferable energy has been taken into account, i.e., $b=\Delta$ for $\Delta<E_m$ and $b=E_m$ for $\Delta>E_m$. However, for $k=\xi/E_m\to 0$, $f_V(x,\Delta)\to f_L(x,\Delta)$. For all practical purposes this limit is already satisfied for protons with kinetic energy greater than 150–200 MeV traversing 300 μm of silicon absorber (Aitken *et al* 1968, Hancock *et al* 1983a). In the following, only the Landau function will be considered.

The modified energy-loss distribution takes into account the effect of distant collisions, namely interactions in which the electron binding energy cannot be neglected. The energy straggling function is given by (Fano 1963, Bichsel and Saxon 1975; see also appendix A of Rancoita and Seidman 1982)

$$f(\Delta,x)=\frac{1}{\sigma\sqrt{2\pi}}\int_{-\infty}^{+\infty} f_L(\Delta,x)\exp[-(\Delta-\varepsilon)^2/2\sigma^2]\,d\varepsilon \tag{4}$$

where Δ is the actual energy loss when a thickness x of material is traversed. The standard deviation of the convolving gaussian is

$$\sigma^2=\delta_2=M_2-M_2'$$

where M_2 and M_2' are the second-order moments of the modified cross section taking into account the effect of electron binding and the Rutherford cross section, respectively. (Bichsel (1970) has shown that further higher moments give negligible contributions.) The value of σ can be computed following Shulek *et al* (1967):

$$\sigma^2=\tfrac{8}{3}\xi\sum_i I_i(Z_i/Z)\ln(2m_e c^2\beta^2/I_i) \tag{5}$$

where I_i is the ionisation potential of the ith shell (Sternheimer 1966), Z_i is the number of electrons in the ith shell of the stopping material and the summation is carried out over those shells for which $I_i<2m_e c^2\beta^2$. In the predictions of Bichsel (1981) and Bichsel and Yu (1972†), the value of σ^2 increases as $\ln\gamma$ for $\beta\to 1$:

$$\sigma^2=2\xi[C_1+C_2(2\ln(\beta\gamma)-\beta^2)]$$

where $C_1\to 6$ keV and $C_2\to 0.29$ keV in silicon for $\beta\to 1$.

The energy loss sensed by a detector is described by equation (4) whereas the convolving gaussian has the standard deviation σ_t given by

$$\sigma_t^2=\sigma^2+\sigma_{noise}^2.$$

σ_{noise} is the standard deviation of the gaussian noise distribution.

If n relativistic particles traverse a detector, we expect that the energy-loss distribution is

$$\Lambda(\Delta,n)=f(\Delta,nx) \tag{6}$$

where $\xi_n=n\xi$, $\sigma_t^2=n\sigma^2+\sigma_{noise}^2$ and $\Delta_{n,mp}=n(\Delta_{mp}+\xi\ln(n))$.

The values of Δ_{mp}, dE/dx (average stopping power) and σ for charged hadrons (π, K,

† In this paper the quantity D/ε_m ($D=\delta_2/2\xi$) has been computed for an incoming proton with kinetic energy between 0.1 and 10 GeV.

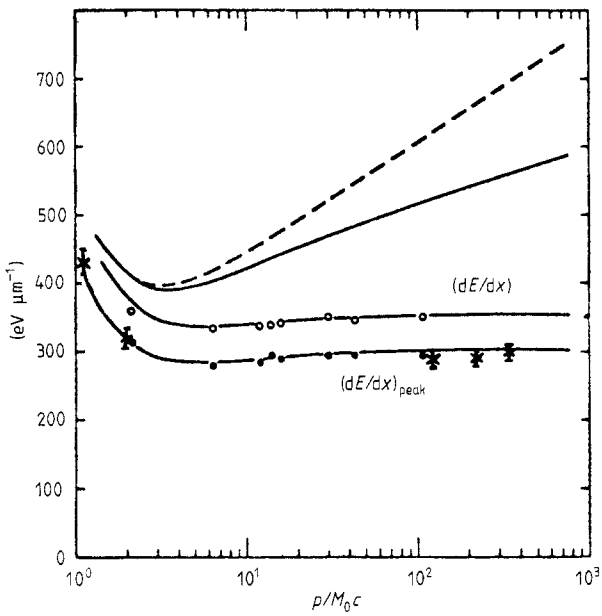

Figure 1. Energy loss in silicon (in eV μm^{-1}) as a function of the parameter $p/M_0c=\beta\gamma$. ●, ○, a 900 μm thick detector (Esbensen *et al* 1978). ×, a 300 μm thick detector (Hancock *et al* 1983a). The curves are (from the top) the average stopping power without (broken curve) and with (full curve) the density effect, the average stopping power with both the restriction (Sternheimer 1971) and the density effect taken into account and the prediction of the most probable energy loss compared with the experimental points.

p) have been investigated in the kinetic energy range between 0.25 and 115 GeV (Esbensen *et al* 1978, Hancock *et al* 1983a). In figure 1 the values of dE/dx and Δ_{mp} are given for $\beta\gamma$ in the range 1.1–336. As expected, no relativistic rise is observed. The agreement with the

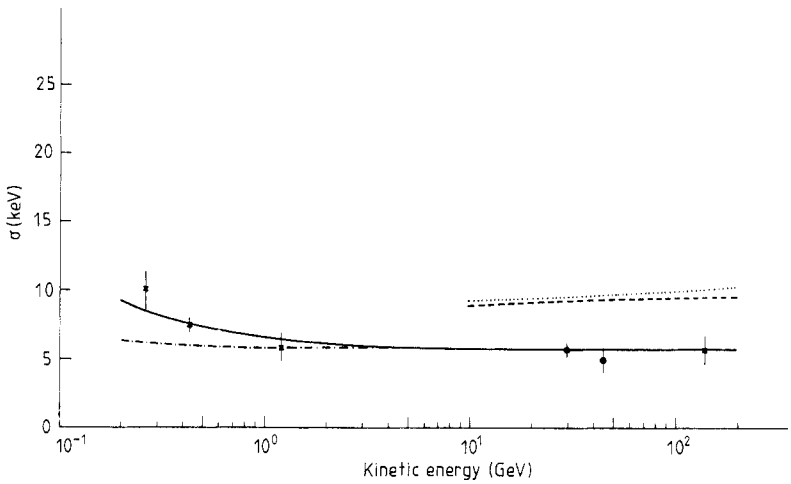

Figure 2. Measured values of the parameter σ (Hancock *et al* 1983a). The full and chain curves are the predictions of Shulek *et al* (1967) for protons and pions, respectively, and the broken and dotted curves are the predictions of Bichsel (1981) for protons and pions, respectively.

Bethe–Bloch formula is satisfactory when both the restriction (Sternheimer 1971) and the density effect are taken into account.

The measured σ values (figure 2 (from Hancock *et al* 1983a)) are in agreement with the predictions of Shulek *et al* (1967) (equation (5)).

In figures 3(*a*) and (*b*) two energy-loss spectra are shown (Hancock *et al* 1983a). The curves are the fitted functions, namely the modified energy-loss distribution given by equation (4). The standard deviation of the noise contribution was measured before the data taking. Its value was approximately 4.0 ± 0.4 keV.

A study of the energy loss of several relativistic particles has been performed at the CERN SPS (Hancock *et al* 1983b). The incoming proton beam had a momentum of 115 GeV/*c*. The final multiplicities were selected in a forward acceptance cone of 2.3° by employing a microstrip detector. In figure 4 a multiparticle spectrum is shown. The single particle (beam particle) constitutes about 41% of the events. The full curve is the fitted curve, in which the free parameters are the values of σ and ξ for the single particle and the relative contents of one, two, three and four particles. In the fitting procedure, the energy-loss distribution of n particles is given by equation (6). There is good agreement between the experimental spectrum and the fitted curve.

3. Microstrip devices

A microstrip detector is a silicon device in which the junction side or the rear side is made from strip electrodes. The strip pitch is the distance between the middle of two adjacent interstrips (see figure 5). Microstrip detectors can at present be made with strip pitch 20 μm and strip length 6 cm.

3.1. Charge sharing and efficiency

The charge sharing (between neighbouring strips) and the efficiency have been investigated for both surface-barrier and ion-implanted silicon detectors (Bonamy *et al* 1981a, b) at the CERN PS. The momentum of the incoming pion beam was 10 GeV/*c*.

The beam particle traversing a surface-barrier detector generated both single- and double-hit events† (the triple-hit events were negligible). In figure 6 (from Bonamy *et al* 1981a) the overall energy loss (including both single- and double-hit events) is shown for a 400 μm thick detector. The charge-sharing effect characteristic of double hits is responsible for the accumulation of events for energies lower than the most probable energy. In fact, the data sample selected requiring single-hit events shows an energy-loss distribution (figure 7(*a*)) which is well represented by equation (4). The percentage of double hits could be related to the interstrip resistance. However, it cannot be easily controlled during the manufacturing process.

The ion-implanted detector did not show any particular double-hit phenomenon. In figure 7(*b*) the overall energy-loss distribution sensed by a strip is given. It is well represented by equation (4). At present most microstrip detectors in common use are ion implanted. Both the ion-implanted and surface-barrier devices had an efficiency compatible with 100% (Bonamy *et al* 1981a, b).

† A single-hit event is defined when a single strip detects a signal greater than $3\sigma_{noise}$ (σ_{noise} is the standard deviation of the gaussian noise distribution). A double-hit event is defined when two neighbouring strips detect signals greater than $3\sigma_{noise}$.

3.2. Capacitive charge-sharing device

A capacitive charge division detector has been developed (Hyams *et al* 1983) in order to reduce the number of read-out channels. In the device: (i) the intermediate strips are kept at

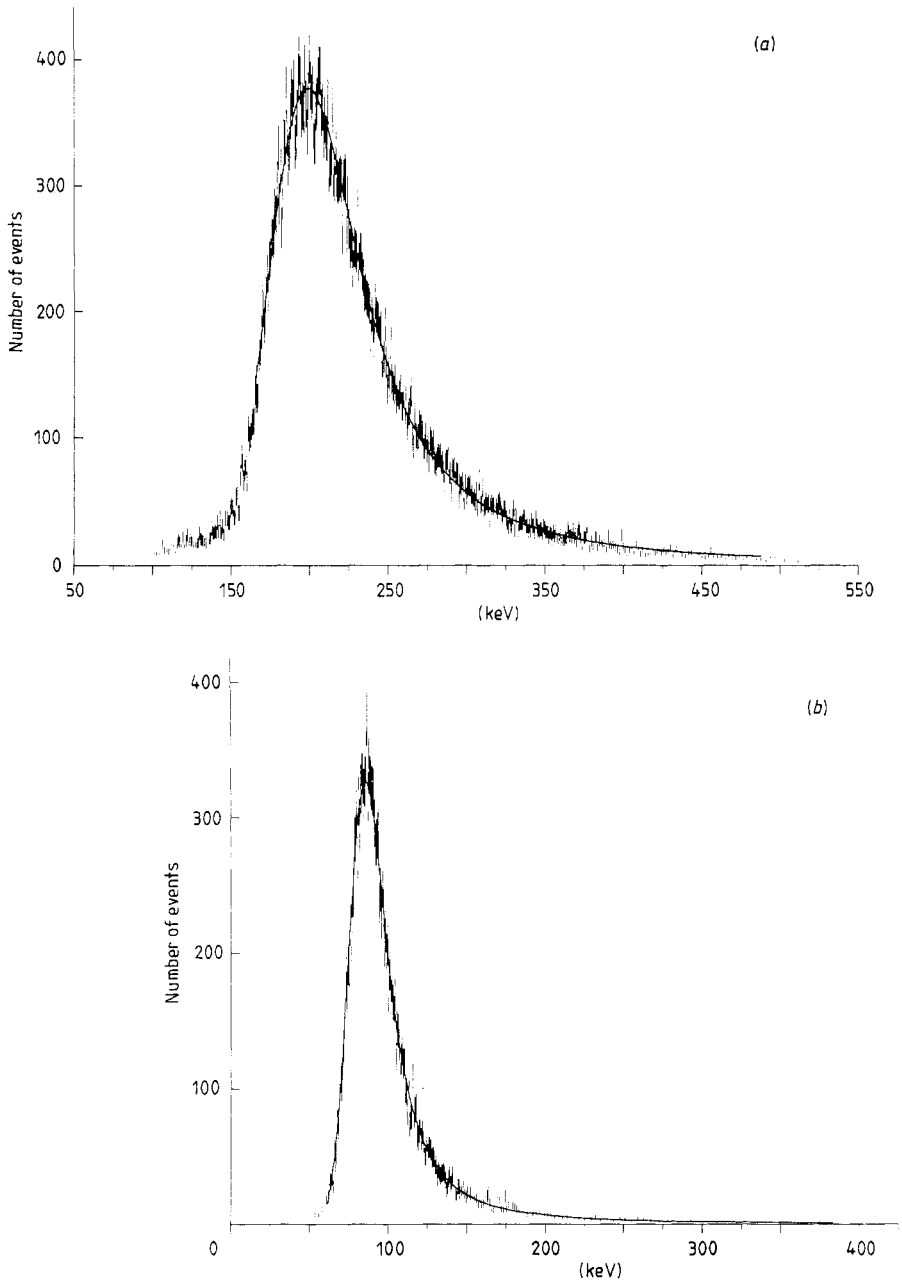

Figure 3. Parts (*a*) and (*b*) show the energy-loss spectra at 0.736 and 115 GeV/*c* incoming proton momenta, respectively. The full curves are the complete fits to the experimental data. The values of ξ are 15.0 ± 0.8 and 5.6 ± 0.3, respectively; the values of σ are 10.2 ± 1.4 and 5.7 ± 1.1, respectively.

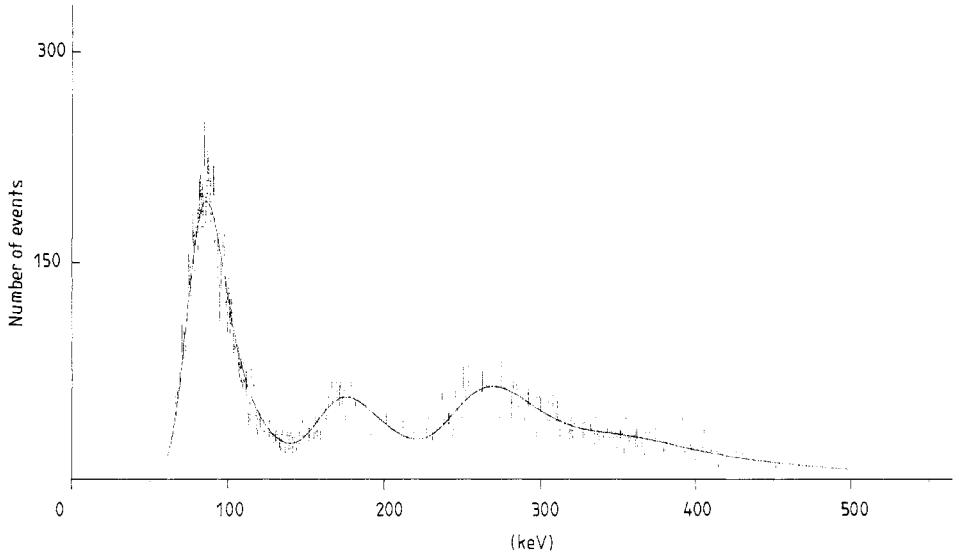

Figure 4. Energy-loss spectrum including both single and several relativistic particles. The percentages, $P(n)$, of the numbers of particles produced are 0.41, 0.19, 0.31 and 0.09 for one, two, three and four particles, respectively. The full curve is the fitted curve.

the same potential as the read-out strips; (ii) the impedance between read-out strips is much greater than the input impedance of the electronics in order to avoid cross-talk; (iii) the interstrip capacitance is greater than the strip-to-ground capacitance. In this way, the charge collected at intermediate strips can be divided amongst the neighbouring read-out strips. The impact position of the incoming particle is found by computing the centre of gravity of the charge collected. The signals from the associated electronics have a base time of about 800 ns.

The detectors made for the NA11 experiment at the CERN SPS have 20 μm pitch strips and a read-out channel every three strips. In this way a spatial resolution of about 5 μm and two-particle separation of 120 μm can be obtained.

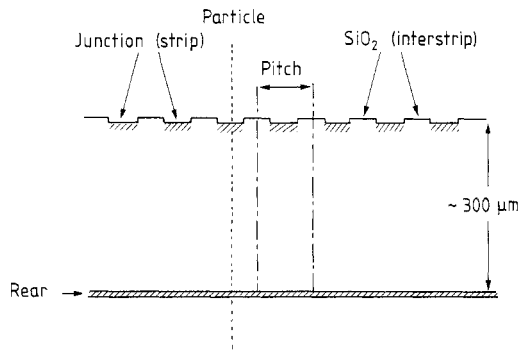

Figure 5. Sectional view of a microstrip detector.

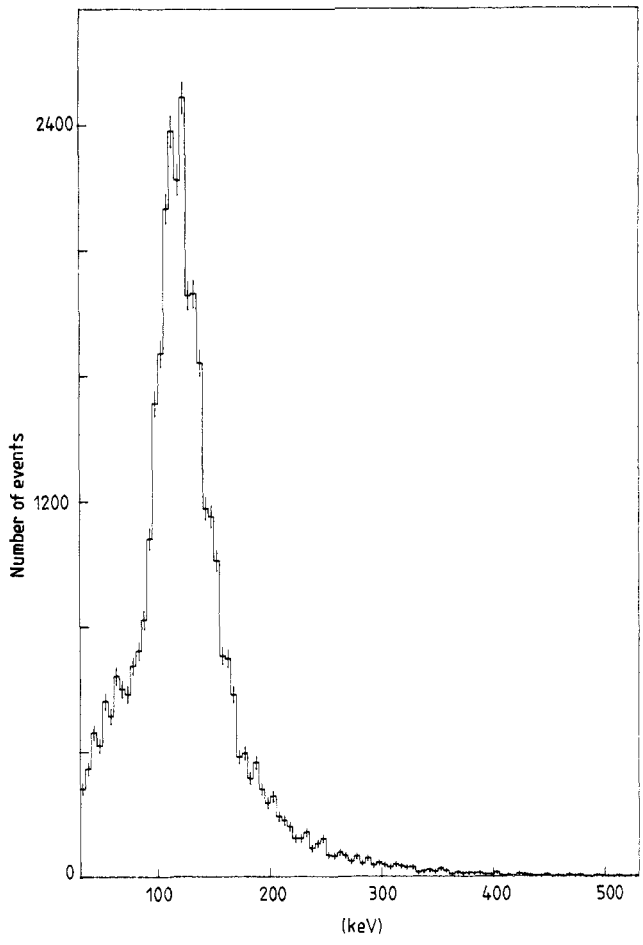

Figure 6. Total energy-loss distribution as sensed by a 400 μm thick and 200 μm strip pitch surface-barrier detector (Bonamy *et al* 1981a).

3.3. Magnetic field effect

The charge collection in a silicon microstrip detector has been investigated by using a 280 μm thick, 20 μm pitch strips device (Belau *et al* 1983) with individual read-out. The strips were oriented horizontally, parallel to the magnetic field and perpendicular to the incoming 200 GeV/c beam. The effects on both hole and electron collection have been studied.

Without magnetic field the charge distribution is symmetric with a FWHM of 6 μm (for holes) at 120 V (figure 8(a)) and which decreases to 4.5 μm at 200 V. The distribution agrees with the expectation from charge diffusion in silicon.

The magnetic field causes the charges to drift at an angle θ_L with respect to the direction of the electric field. The value of the drift angle is expected to be

$$\tan(\theta_L) = \mu_H H \times 10^{-4}$$

where μ_H is the Hall mobility† and H is the magnetic field in T.

† Typical values of μ_H are 310 cm^2 V^{-1} s^{-1} for holes and 1650 cm^2 V^{-1} s^{-1} for electrons.

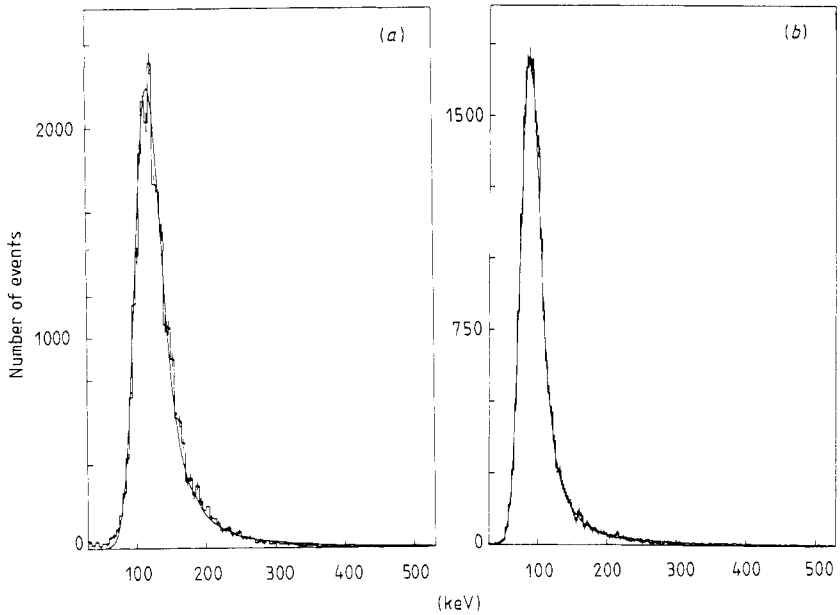

Figure 7. Single-hit energy-loss distribution. The full curves represent the fitted distributions (Landau distribution convolved by a gaussian function, equation (4)): (*a*) 400 μm thick and 200 μm strip pitch surface-barrier detector; (*b*) 300 μm thick and 200 μm strip pitch ion-implanted detector.

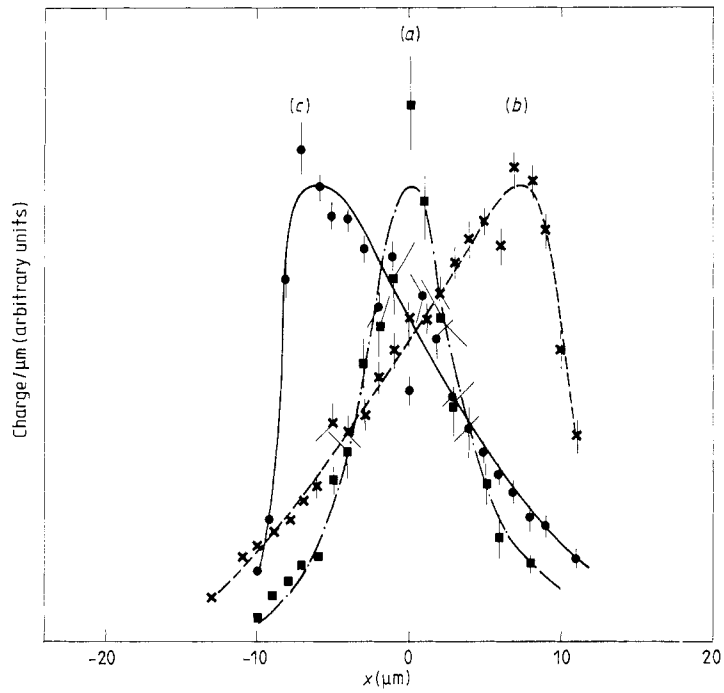

Figure 8. Collected charge (hole) distribution (Belau *et al* 1983): (*a*) no magnetic field applied; (*b*) with a magnetic field of 1.68 T; (*c*) with a magnetic field of −1.68 T. The full curves are the fitted charge distributions.

A systematic shift of the measured coordinate of about 10 μm (for holes) and an increase in the width of the collected charge distribution to about 12 μm (figures 8(*b*) and (*c*)) was observed by applying a magnetic field of 1.68 T. The mean expected shift of 7.3 μm (37.9 μm) for holes (electrons) was in agreement with the measured one (Belau *et al* 1983).

4. Applications of silicon detectors to high-energy physics

Important technological developments regarding silicon detectors were started after experimental evidence for the short-lived $D\bar{D}$ particle production was observed. These developments have allowed the use of highly compact multilayer targets. Sets of microstrip devices are now currently located downstream of the target in experiments searching for charm and beauty. Such devices look attractive for colliding beam machine experiments. Therefore large-scale integration (LSI) preamplifier chips and large-area silicon detectors for calorimetry applications are currently being investigated.

4.1. Fixed-target experiments

4.1.1. The NA1 experiment. A measurement of the D^+D^- lifetime has been proposed (and performed) at the NA1 photoproduction experiment at the CERN SPS. The target was an active multilayer silicon detector. Incoming photons whose energies were greater than about 100 GeV produced the $D\bar{D}$ system on silicon coherently. At these energies, the two particles had a mean decay path of a few millimetres in the laboratory. Thus the target, consisting of 40 detectors (300 μm thick and spaced by 150 μm) could either select coherent reactions or detect a multiplicity step at the decay position† of the short-lived particles (Albini *et al* 1982a, b).

A total of 86 D^+D^- candidates‡ were selected by requiring that (i) $M_1 + M_2$ (M_i is the reconstructed mass of the charmed particle) is between 3.66 and 3.90 GeV/c^2 and (ii) a coherent signal is followed by a multiplicity level of two and one or two steps (figure 9).

Unfortunately, an unambiguous identification of the final state could not be obtained because no tracking microstrip device was associated with the target. It was assumed that

$$\gamma_{D^+} = \gamma_{D^-} = E(\text{energy of the incoming photon})/2m_{D^\pm}$$

where $m_{D^\pm}$ is the mass of the $D^\pm$ meson and $\gamma_{D^\pm}$ is the Lorentz factor.

The time distribution of the decays is shown in figure 10 (Albini *et al* 1982a, b). The background contamination (mainly γ-ray conversions) was estimated to be about 10%. Steps due to D^0 decays were evaluated to be about 20%. An overall fit to the data taking these two contributions into account gave

$$\tau_{D^\pm} = 9.5^{+3.1}_{-1.9} \times 10^{-13} \text{ s}.$$

4.1.2. The NA11 experiment. For the heavy flavour program of the NA11 experiment (ABCCMR Collaboration 1982) at the CERN SPS, the silicon high-resolution vertex detector is the major instrument.

The beam telescope consists of six planes of microstrip detectors (figure 11(*a*)). The first four have horizontal strips of pitch 50 μm arranged in pairs staggered by 25 μm. The

† The reconstruction procedure is explained in § 2.

‡ A detailed discussion of the data analysis is given by Albini *et al* (1982a, b) and Bellini *et al* (1982).

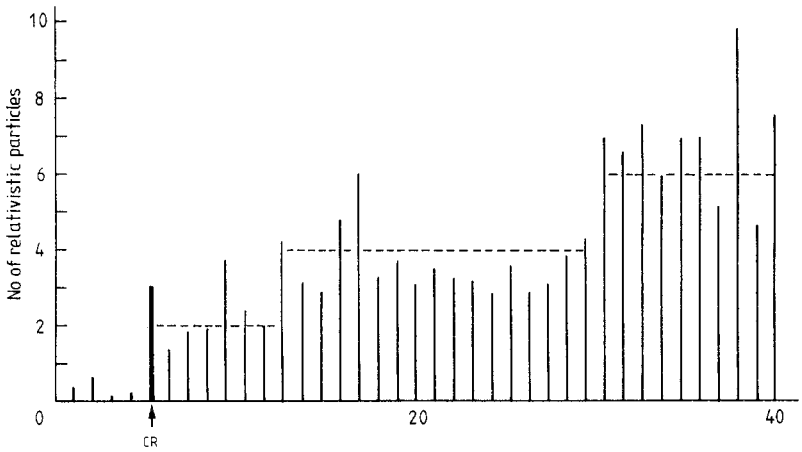

Figure 9. Energy loss (in number of relativistic particles) for a candidate D^+D^- event photoproduced coherently on Si, as sensed by the NA1 active target (Albini *et al* 1982a, b). Each detector is 300 μm thick and the spacing (along the beam direction) between the detectors is 150 μm. CR indicates the signal corresponding to a recoiling Si nucleus; its energy loss is consistent with a coherent reaction.

last two have strips aligned at $\pm 14°$ to the horizontal and are of pitch 20 μm. The impact position of the incoming 200 GeV/c π^- particle is measured with a precision of 5 μm vertically and 20 μm horizontally. A strong focusing mode provides a beam full width of 250 μm vertically and 15 mm horizontally.

The active target consists of 10 planes of silicon counters 280 μm thick and spaced at 500 μm intervals along the beam direction (figure 11(*b*)). They have horizontal strips of pitch 20 μm and length 26 mm. Two more Si detectors with strips of pitch 400 μm are located 20 mm downstream. The output pulses from the associated shaping amplifiers are

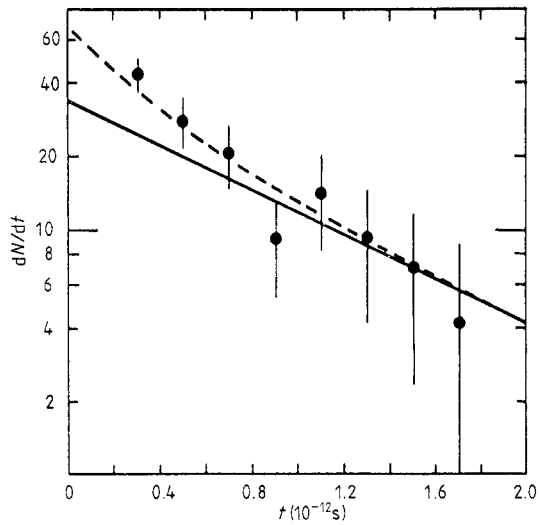

Figure 10. Time distribution of identified charmed-particle decays. The full curve gives the $D^{\pm}$ contribution and the broken curve is the overall fit to the data taking a D^0 contamination of the order of 20% into account (Albini *et al* 1982a, b).

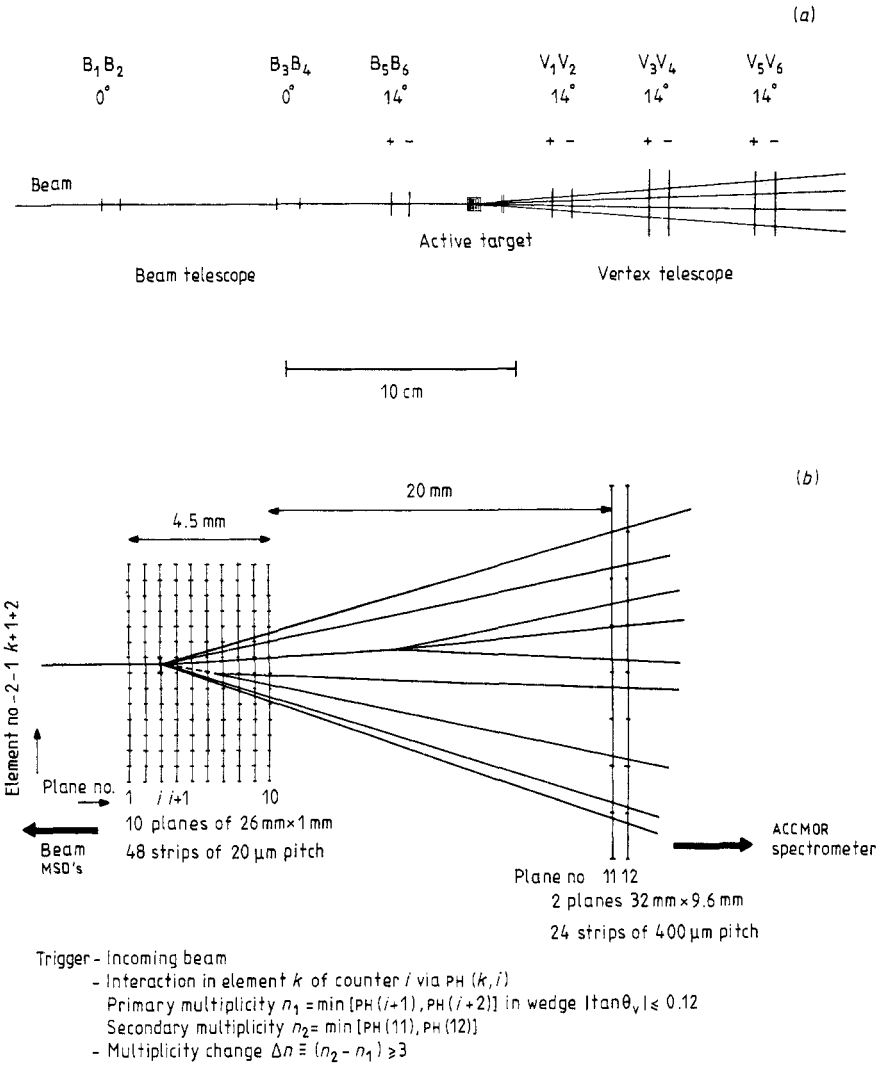

Figure 11. (*a*) Lay-out of the NA11 vertex telescope. The silicon detectors B_1–B_4 have horizontal strips of pitch 50 μm. The silicon detectors B_5 and B_6 have strips with pitch 20 μm and are aligned at $\pm 14°$ to the horizontal. The devices V_1–V_6 are capacitive charge-division detectors. Their resolution is 5 μm and they have strips inclined at $\pm 14°$ to the horizontal. (*b*) Lay-out of the NA11 active target: 10 planes of silicon detectors with 20 μm pitch strips and spaced at 500 μm intervals along the beam. Two microstrip detectors with 400 μm pitch strips are located 20 mm downstream.

digitised within 10 μs. The information is used by a microprocessor to provide the trigger. The aim is to measure the primary and secondary multiplicities in a narrow forward cone of about 7°. A charm candidate is accepted if there is a multiplicity change of four.

The vertex telescope (figure 11(*a*)) consists of six silicon strip counters of thickness 280 μm and sensitive area 24×36 mm^2. They are capacitive charge division detectors (§ 3.2) and measure one projection with 5 μm resolution. The six planes are arranged in two views of $\pm 14°$ inclination to the horizontal. They allow (i) a precise reconstruction of

both the primary and secondary vertices and (ii) a considerable reduction in the combinatorial background.

4.1.3. The NA14 experiment. This experiment (ACLOPPSSSW Collaboration 1982) uses the high-intensity tagged photon beam at the CERN SPS. The primary electron beam intensity is about 2×10^8 electrons/burst with a momentum of 175 GeV/c.

The target is a multilayer silicon detector (figure 12). There are 30 planes, each 300 μm thick and spaced by 200 μm. Each plane has an active area of 20 cm^2 and is split into 24 vertical strips of width 2 mm. A 31st detector with horizontal strips is added downstream. A set of four microstrip doublets is located after the target. Each doublet is spaced by 1.5 cm and the first one is 1.5 cm from the multilayer silicon detector. The first three doublets have the strips oriented vertically and horizontally. The fourth one has the strips at $\pm 15°$ to the horizontal. Each detector has an active area of 5×5 cm^2 and a strip pitch of 50 μm. Fast electronics ($\approx$40 ns of signal base time) are associated with both the multilayer target and the microstrip detectors. In this way the active vertex can stand the very high counting rate due to the electromagnetic background. The counting rate in each strip of the last target layer is approximately 5×10^5 counts/2 s burst.

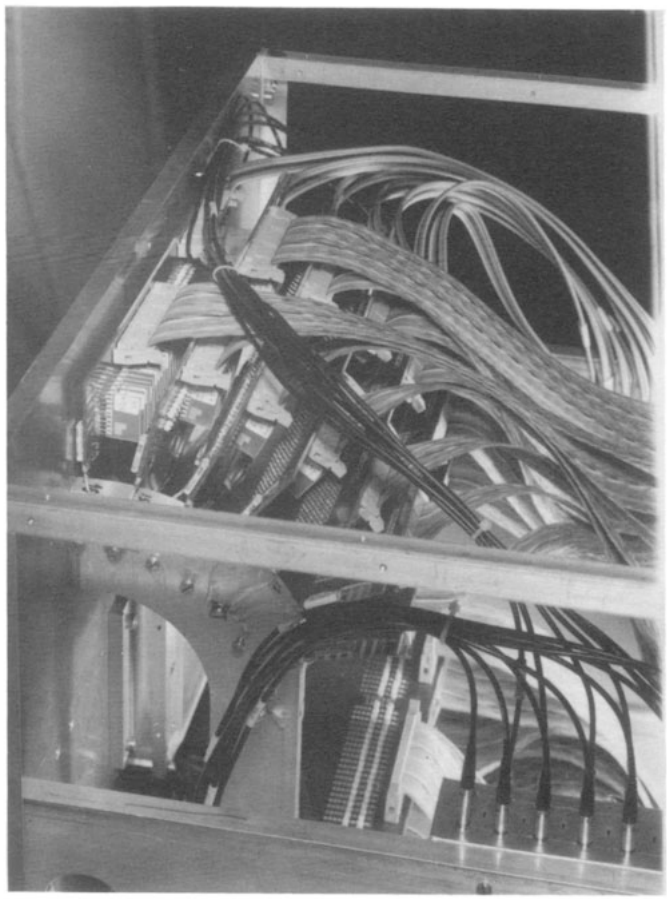

Figure 12. Side view of the NA14 multilayer silicon target. Each layer, 300 μm thick, is split into 24 detectors of width 2 mm. The strips are vertical. The beam is coming from the right.

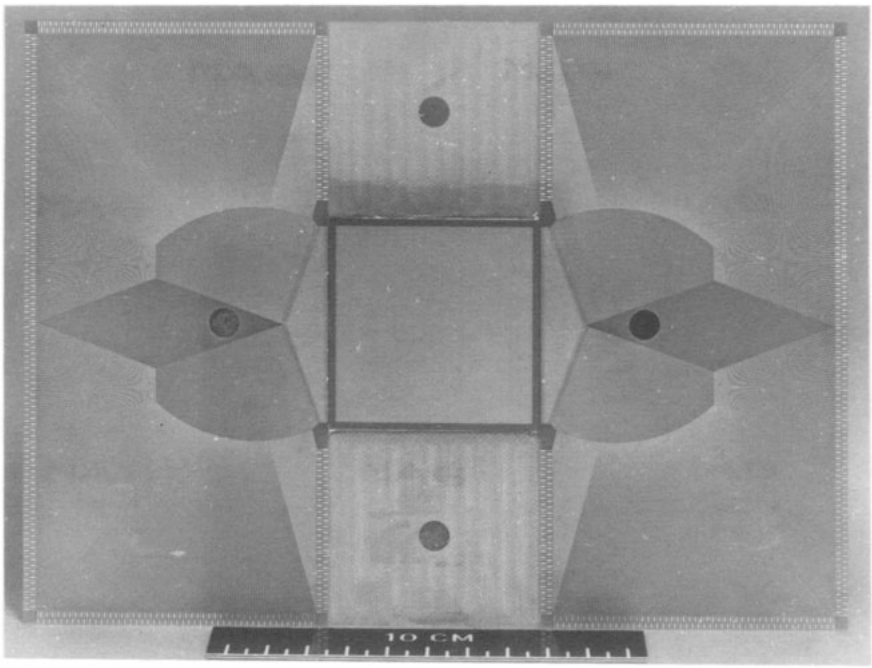

Figure 13. Microstrip detector with active area of 5×5 cm^2. The strip pitch is 50 μm. Each strip is connected to fast electronics with $\approx$15 ns rise time and $\approx$25 ns fall time of the signal.

The experiment will start taking data on heavy flavour photoproduction during 1984. The information from the silicon vertex detector will be used off-line (i) for selecting the charm candidates, (ii) for localising the decay vertices and (iii) for associating the tracks with their correct vertices. The filtering procedure flags a charmed-meson candidate when off-set tracks† are obtained from the reconstruction in the microstrip detectors and one or two steps in multiplicity are detected in the multilayer target. A sample of about 50–200 fully reconstructed charmed events per decay channel is expected.

The multilayer target has already been tested. A tungsten dump with a length of 85 cm was located downstream of the device. The trigger was formed by requiring that an incident photon interacts in the target and that one or two muons emerge from the dump. In this way an enriched charm sample was expected. The active target worked satisfactorily, except for four unbiased layers. In figure 14 an event with a multiplicity step is shown. The interaction layer has sensed an energy loss compatible with that expected for the coherent recoil of a silicon nucleus. The following layers detect two and the others four relativistic particles. On the left side the height corresponding to the most probable energy loss of 10 relativistic particles is given. The spurious hits around the interaction are due to the electromagnetic background.

4.1.4. Hybrid experiments. Some fixed-target experiments (table 2) are planning to employ a hybrid technique, namely an emulsion target followed by microstrip detectors (CGMMPR Collaboration 1981 (experiment WA71 at the CERN SPS), BBCDKKLNNRTUY Collaboration 1981 (experiment WA75 at the CERN SPS), Reay

† An off-set track is at more than about 80 μm from the interaction vertex. The track is reconstructed by using the data from the microstrip detectors.

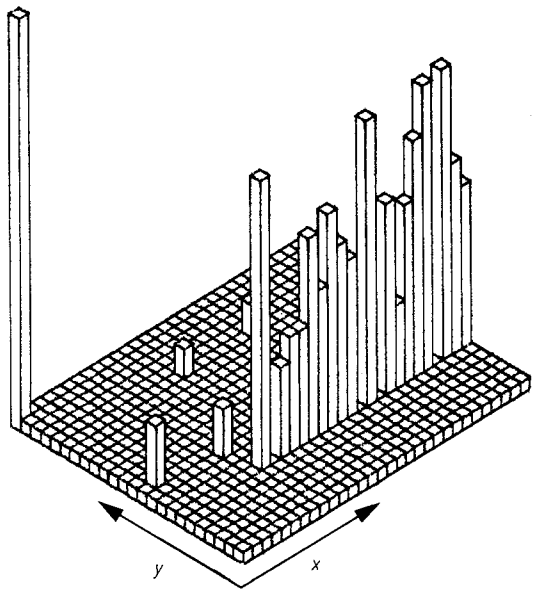

Figure 14. Multiplicity step sensed by the NA14 multilayer target. The y axis is 4 cm long and the x axis is 1.5 cm long. On the left the energy loss corresponding to 10 relativistic particles is given.

1981 (experiment E653 at Fermilab)). The silicon counters provide a resolution of about 10 μm in the plane of the emulsion sheets and about 200 μm along the beam direction. They locate the interaction vertex and off-set tracks and allow a substantial improvement in the identification of events in the emulsion. Therefore it is possible to reduce the number of events to be scanned. The charmed or beauty particle candidate is decided by observing the decay vertex in the emulsion. Usually a beam hodoscope consisting of silicon detectors gives the impact coordinates on the target.

In the WA71 experiment at the CERN SPS, two multilayer silicon detectors are placed in between the target and the set of microstrip devices. An on-line pulse-height analysis is performed. The multiplicity of one event is measured at two distances, i.e. at 1 mm and 10 mm, from the target. The event is triggered if a step in multiplicity greater than or equal to two is detected.

Table 2. Hybrid experiments employing silicon detectors for hadroproduction of heavy flavours.

Approved experiment	Associated microstrip detectors	Silicon detectors in trigger
WA75	7 planes, 300 μm thick, 50 μm pitch and 6 planes for the beam hodoscope	
WA71	6 planes, 400 μm thick, 50 μm pitch and 2 planes for the beam hodoscope	Step in multiplicity detected by 2 silicon multilayer telescopes
E653	21 planes, 300 μm thick, 40 μm pitch and 9 planes for low-angle track measurement	

In general the hybrid technique can achieve a better identification of charm event candidates. However its main limitation comes from the number of events which can actually be scanned.

4.2. Colliding beam machine experiments

At the very high energy at which an interaction occurs in the present and forthcoming colliding beam machines, silicon detectors can provide a well suited high-resolution vertex detector. Thus a separation of the heavy flavour decay vertices from the interaction vertex is achievable. Furthermore it improves the momentum resolution of the central detector. The construction of a large-area mosaic of detectors does not seem to have too many difficulties. However the high resolution is thought to be obtained by the individual read-out of strips of very fine pitch ($\approx 25\ \mu$m). In § 4.2.1, a project in which a 'microplex' read-out chip is under investigation is described.

Silicon detectors can find application in calorimetry as the active sampling layer. They operate in magnetic environments, where there are geometric constraints, or in vacuum. Large-size inexpensive devices are manufactured by using low-resistivity ($\approx 1500\ \Omega$ cm) material. Although the counter works as undepleted device, in calorimetry a sensitive volume of about 50% of the physical one is sufficient due to the large number of traversing particles.

4.2.1. Microvertex and large-scale integration. The proposed microvertex for the DELPHI experiment at the LEP (Bosman *et al* 1983) consists of three concentric cylinders of silicon wafers. The radius of the inner cylinder is 8–9 cm and is close to the vacuum pipe. An assembly of 30 unit 'cells', on average, builds up a cylinder (figure 15). A cell consists of an open quartz frame onto which are glued (i) 7 detectors, each with an active area of $6 \times 2.5\ \text{cm}^2$ and a thickness of 300μm, (ii) 10 read-out chips, each with an area of $0.4 \times 0.6\ \text{cm}^2$ and a thickness of $380\ \mu$m and (iii) 10 (or less) driver chips, each with an area of $0.4 \times 0.5\ \text{cm}^2$ and a thickness of $380\ \mu$m. The microstrip detectors are interconnected by wire bonding. The strip pitch is $25\ \mu$m.

The 'microplex' read-out is still under computer design. The technology is standard, but the design is unusual, combining large-scale integration (LSI) with low noise. It is

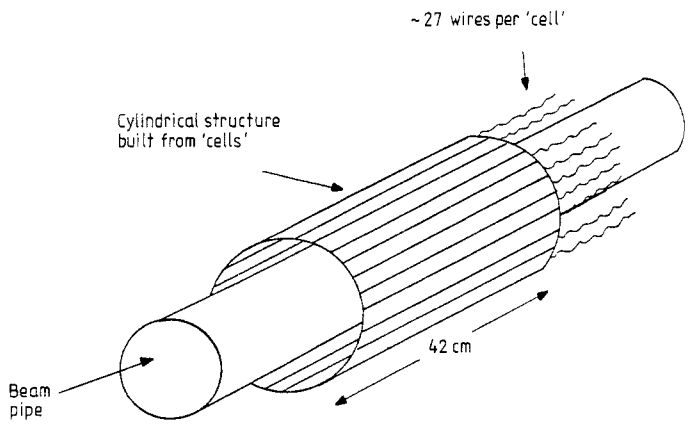

Figure 15. Lay-out of one silicon cylinder of the proposed microvertex for the DELPHI experiment at the LEP.

expected to have an excellent noise performance, i.e. the gaussian noise distribution has a standard deviation $\sigma \approx 4$ keV. The rise time of the amplifier signal is approximately 10 ns. Every chip has 128 channels.

4.2.2. Silicon detectors and calorimetry. Silicon detectors can be used in sandwich calorimeters as active sampling layers. Due to the small amount of energy necessary to create an e–h pair (≈ 3.6 eV), very compact calorimeters can be built up. They may work at room temperature and their electronics are easily accommodated nearby.

The large-size active areas are achieved by employing inexpensive, low-resistivity material (Barbiellini and Rancoita 1983), cut to a standard thickness of approximately 300 μm. Thus, as mentioned above, the detectors work as undepleted devices. In actual practice, the sensitive region is the charge-depletion layer plus an additional region, the thickness of which is a fraction of a carrier diffusion length,

$$L = (D\tau)^{1/2},$$

where D is the diffusion coefficient† of the minority carriers, i.e. the holes in n-type bulk silicon, and τ is the minority carrier lifetime. In the case of relativistic particles traversing an undepleted detector, only minority carriers created by the energy lost in a region of approximate thickness 6 μm may migrate from the field-free region into the space-charge region. For n-type silicon, the depleted space-charge region is

$$d = 0.53(\rho V)^{1/2} \ \mu\text{m}$$

where ρ is the resistivity in Ω cm and V is the applied reverse bias. As an example, a detector made using a 1500 Ω cm wafer has a depleted layer approximately 160 μm thick at 60 V of reverse bias.

To prove the feasibility of using undepleted detectors, a test was performed on an ion-implanted detector of resistivity 7 kΩ cm, thickness 300 μm and active area 1×1 cm^2 using a 30 GeV/c pion beam at the CERN SPS (Barbiellini and Rancoita 1983). At any applied voltage lower than that required for full depletion, the resulting energy-straggling spectrum sensed by the detector was in agreement with the modified energy-loss distribution (equation (4)) of a relativistic particle traversing a silicon absorber of thickness equal to that of the depleted layer. In figures 16(*a*) and (*b*) the energy-loss spectra obtained at 55 and 10 V are shown. The corresponding depleted layers were 300 μm (fully depleted) and approximately 200 μm, respectively. The full curves are the fits to equation (4) including the gaussian noise contribution.

In a silicon sandwich calorimeter, the energy resolution is limited only by the sampling fluctuations due to the silicon density. Thus using tungsten as showering material, the expected energy resolution (Amaldi 1981) for a contained shower, fully depleted silicon and one sampling per radiation length is approximately $9.2\%/\sqrt{E}$. The total energy is contained in a cylinder having a radius of about 1.8 cm. About 26 radiation lengths are necessary to contain the longitudinal shower development for incoming electron energies up to 50 GeV. The physical length of this sandwich calorimeter is about 10 cm.

At present silicon/lead or silicon/tungsten calorimeters are likely to be built as the LEP luminosity monitor and the forward electron tagger at the HERA machine. In both cases a set of microstrip detectors is located upstream in order to track the incoming electron. They are supposed to be placed around the beam pipe.

† The diffusion coefficient is $D = \mu kT/e$ where k is the Boltzmann constant, T is the absolute temperature, e is the electron charge and μ is the carrier mobility.

A prototype of the silicon/tungsten calorimeter will be tested at the X7 electron beam at the CERN SPS, starting in the summer of 1983. It consists of 15 tungsten layers, each

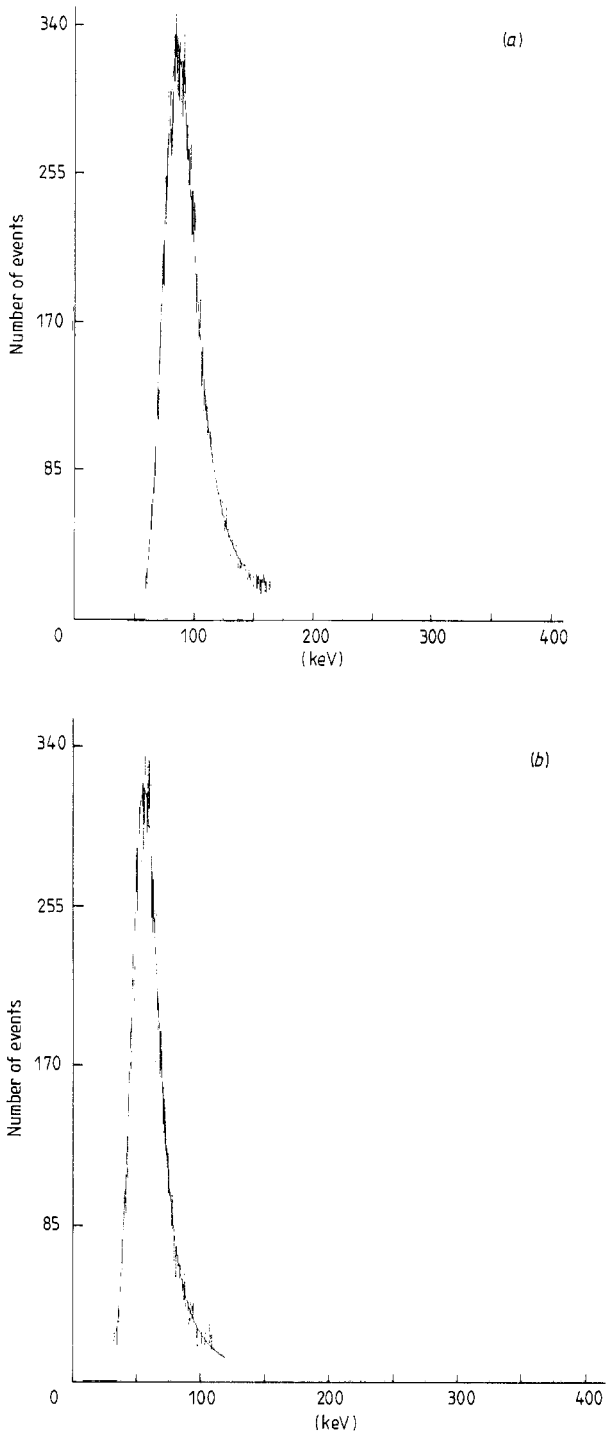

Figure 16. (*a*) Energy the loss of a relativistic pion traversing a 300 μm Si detector. The applied reverse bias is 55 V corresponding to that necessary for full depletion. The full curve is the best fit to a Landau distribution convolved by a gaussian. The most probable energy-loss is 83.8 ± 4.2 keV. The FWHM of the Landau distribution is 23.1 ± 1.2 keV. The FWHM of the gaussian (with the noise contribution subtracted) is 13.2 ± 0.7 keV. (*b*) Energy loss of a relativistic pion traversing a 300 μm Si detector. The applied reverse bias is 10 V. The detector is operating as an undepleted detector. The full curve is the best fit to a Landau distribution convolved by a gaussian. The most probable energy loss is 53.2 ± 2.7 keV. The FWHM of the Landau distribution is 16.7 ± 0.8 keV. The FWHM of the gaussian (with the noise contribution subtracted) is 11.4 ± 0.6 keV.

one of two radiation lengths and interspaced with a 5×5 cm^2 low-resistivity ($\approx$1500 Ω cm) silicon detector as the active sampling layer.

5. Conclusion

Silicon detectors have been used in high-energy physics for 15 years. However spectacular advances have occurred in the past three years.

Complex detector configurations are now possible for heavy flavour fixed-target experiments. They have microstrip detectors downstream of the target. This target may consist of multilayer silicon or emulsion sheets. The secondary vertices can be located with a precision of a few hundred microns by analysing the energy-loss data when a silicon target is used.

Large-area detectors are proposed as the microvertex in colliding beam machine experiments. They are well suited as high-resolution inner detectors for untangling decay vertices of heavy flavours produced and to improve the momentum resolution of the central detector. A great deal of technological development is currently oriented towards producing large-scale integration preamplifier chips.

Silicon detectors find application in calorimetry as the dense active sampling layer. The calorimeter energy resolution is limited only by the sampling fluctuations. Large-area devices are built by using inexpensive low-resistivity detectors, which operate as undepleted counters. Their sensitive region is given by both the charge depletion layer and a few microns in the field-free region.

Acknowledgments

The author is particularly indebted to Professor A Seidman for his suggestions and for reading and correcting the manuscript. Useful discussions with P Borgeaud, I Siotis, D Treille and D Websdale are gratefully acknowledged.

References

ABCCMR (Amsterdam–Bristol–CERN–Cracow–Munich–Rutherford) Collaboration 1982 Investigation of charm production in hadronic interactions using high-resolution silicon detectors (*CERN/SPSC/82-57 SPSC/P180*)

ACLOPPSSSW (Athens–CERN–London (Imperial College)–Orsay–Palaiseau (Ecole Polytechnique)–Paris (College de France)–Saclay–Southampton–Strasbourg–Warsaw) Collaboration 1982 A program of heavy flavour photoproduction (*CERN/SPSC/82-73 SPSC/P109 Add.2*)

Aitken D W, Lakin W L and Zulliger H R 1968 *Phys. Rev.* **179** 393

Albini E *et al* 1982a Electronic measurement of the lifetime of D^+ mesons (*CERN-EP/82-12*)

—— 1982b *Phys. Lett.* **110B** 339

Amaldi U 1981 *Phys. Scr.* **23** 408

Barbiellini G and Rancoita P G 1983 A luminosity monitor for LEP using electromagnetic calorimeters: the silicon/lead sandwich (*CERN-EP Internal Report 83-01*)

BBCDKKLNNRTUY (Bari–Brussels–CERN–University College Dublin–Kariya–Kobe–University College London–Nagoya University–Nagoya Institute–Roma–Torino–Utsunomiya–Yokohama) Collaboration 1981 An experiment to observe directly beauty particles selected by muonic decay in emulsion to estimate their lifetimes (*CERN/SPSC/81-69 SPSC/P-166*)

Belau E *et al* 1983 *Nucl. Instrum. Methods* **214** 253

Bellini G, Foà L and Giorgi M 1982 *Phys. Rep.* **83** 9

Bichsel H 1970 *Phys. Rev.* B **1** 2844
—— 1981 Private communication
Bichsel H and Saxon P 1975 *Phys. Rev.* A **11** 1286
Bichsel H and Yu S 1972 *IEEE Trans.* **NS-19** 172
Boersch-Supan W 1961 *J. Res. Natl Bur. Stand.* **65B** 245
Bonamy P, Borgeaud P, Movchet J and Rancoita P G 1981a Performance of surface-barrier and ion-implantation silicon detectors (*CERN-EP Internal Report 81-06*)
—— 1981b *Proc. Semiconductor Detector Workshop, Fermilab, 15–16 October 1981* ed. T Ferbel p 257
Borgeaud P, McEwen G, Rancoita P G and Seidman A 1983 *Nucl. Instrum. Methods* **211** 363
Bosman M, Hyams B, Weilhamer, P and Zalewska A 1983 *DELPHI Vertex Detector Note #1, DELPHI group note*
CGMMPR (CERN–Genoa–Milan–Moscow–Paris (LPNHE)–Rome) Collaboration 1981 An experiment for studying beauty production and lifetime in the upgraded Ω′ spectrometer (*CERN/SPSC/81-18 SPSC/P159*)
Esbensen H *et al* 1978 *Phys. Rev.* B **18** 1039
Fano U 1963 *Ann. Rev. Nucl. Sci.* **13** 1
Hancock S, James F, Movchet J, Rancoita P G and Van Rossum L 1983a *Phys. Rev.* A **28** 615
—— 1983b Energy-loss distributions for single and several particles in a thin silicon absorber (to appear in *Nucl. Instrum. Methods*)
Heijne E 1981 Radiation damage: experience with silicon detectors in high-energy beams at CERN (*CERN EF-BEAM 81-6*)
Hyams B, Koetz W, Beau E, Klanner R, Lutz G, Neugebauer E, Wylie A and Kemmer J 1983 *Nucl. Instrum. Methods* **205** 99
Landau L 1944 *J. Phys. (USSR)* **8** 201
Rancoita P G and Seidman A 1982 *Riv. Nuovo Cimento* **5** no 7 and references therein
Reay N M 1981 A proposal to measure charm and B via hadronic production in hybrid emulsion spectrometer (*Fermilab Report*)
Shulek P, Golovin B M, Kulyukina L A, Medved S V and Pavlovich P 1967 *Sov. J. Nucl. Phys.* **4** 400
Sternheimer R M 1966 *Phys. Rev.* **145** 247
—— 1971 *Phys. Rev.* B **3** 3681
Vavilov P V 1957 *Sov. Phys.–JETP* **5** 749